AGU PUBLICATIONS

Water Resources Research

RESEARCH ARTICLE
10.1002/2014WR015320

Key Points:
- Contrasting field-scale permeability values are upscaled to a regional context
- Multiscale geophysics assist with equivalent permeability distribution
- Different levels of upscaling are evaluated with finite element flow modeling

Correspondence to:
N. E. M. Dickson,
ndickson03@qub.ac.uk

Citation:
Dickson, N. E. M., J.-C. Comte, J. McKinley, and U. Ofterdinger (2014), Coupling ground and airborne geophysical data with upscaling techniques for regional groundwater modeling of heterogeneous aquifers: Case study of a sedimentary aquifer intruded by volcanic dykes in Northern Ireland, *Water Resour. Res.*, *50*, 7984–8001, doi:10.1002/2014WR015320.

Received 18 JAN 2014
Accepted 6 SEP 2014
Accepted article online 12 SEP 2014
Published online 16 OCT 2014

Coupling ground and airborne geophysical data with upscaling techniques for regional groundwater modeling of heterogeneous aquifers: Case study of a sedimentary aquifer intruded by volcanic dykes in Northern Ireland

Neil Edwin Matthew Dickson[1], Jean-Christophe Comte[1,2], Jennifer McKinley[3], and Ulrich Ofterdinger[1]

[1]School of Planning, Architecture and Civil Engineering, Queen's University Belfast, Belfast, UK, [2]School of Geosciences, University of Aberdeen, Old Aberdeen, UK, [3]School of Geography, Archaeology and Paleoecology, Queen's University Belfast, Belfast, UK

Abstract In highly heterogeneous aquifer systems, conceptualization of regional groundwater flow models frequently results in the generalization or negligence of aquifer heterogeneities, both of which may result in erroneous model outputs. The calculation of equivalence related to hydrogeological parameters and applied to upscaling provides a means of accounting for measurement scale information but at regional scale. In this study, the Permo-Triassic Lagan Valley strategic aquifer in Northern Ireland is observed to be heterogeneous, if not discontinuous, due to subvertical trending low-permeability Tertiary dolerite dykes. Interpretation of ground and aerial magnetic surveys produces a deterministic solution to dyke locations. By measuring relative permeabilities of both the dykes and the sedimentary host rock, equivalent directional permeabilities, that determine anisotropy calculated as a function of dyke density, are obtained. This provides parameters for larger scale equivalent blocks, which can be directly imported to numerical groundwater flow models. Different conceptual models with different degrees of upscaling are numerically tested and results compared to regional flow observations. Simulation results show that the upscaled permeabilities from geophysical data allow one to properly account for the observed spatial variations of groundwater flow, without requiring artificial distribution of aquifer properties. It is also found that an intermediate degree of upscaling, between accounting for mapped field-scale dykes and accounting for one regional anisotropy value (maximum upscaling) provides results the closest to the observations at the regional scale.

1. Introduction

1.1. Aquifer Heterogeneity

In highly heterogeneous aquifer systems, due to the incomplete understanding of the geological structures, the heterogeneity is often neglected or simplified; a component occasionally necessary for conceptualization. The inherent heterogeneity of geological units is the result of an environments formation process [*Klingbeil et al*., 1999]. As a result, densely measuring heterogeneity is submitted to practical difficulties, commonly excluding 3-D high-resolution sampling of the subsurface, particularly at regional scale. Although acceptable for initial conceptual models, when applied to numerical groundwater models, these generalizations create the potential for unrealistic and unreliable model output. It is important that models include geologically realistic subsurface characterizations [*Chen et al*., 2003] at the appropriate scale. Geophysical data can assist subsurface characterization, however their use can be challenging as they are commonly collected at a smaller scale than they will be modeled [*Wen and Gómez-Hernández*, 1996]. Therefore, modeling requires approaches that account for local heterogeneity while accurately presenting this information on a larger regional scale, i.e., upscaling [*de Marsily et al*., 2005; *Koltermann and Gorelick*, 1996; *Webb and Anderson*, 1996]. In this context, the local heterogeneity refers to intrusive volcanic dykes of low permeability and the values to be upscaled are hydraulic conductivity, *K*.

1.2. Equivalence and Upscaling Techniques in Heterogeneous Media

Equivalent *K* can also be called upscaled [*Renard and de Marsily*, 1997] or block [*Wen and Gómez-Hernández*, 1996] *K* and is defined as the large-scale realization of a constant permeability tensor taken to represent a

heterogeneous medium [*Renard and de Marsily*, 1997]. This methodically combines a large number of facies unit volumes (cells) to create a single larger volume [*de Marsily et al*., 1998], i.e., combining measurement scale cells to obtain a larger, modeling scale cell [*Anderson et al*., 1999; *de Marsily et al*., 2005; *Wen and Gómez-Hernández*, 1996]. This equivalence is achieved through spatial averages [*Renard et al*., 2000]. *Wen and Gómez-Hernández* [1996] and *Renard and de Marsily* [1997] are two primary works that review upscaling and equivalence techniques in hydrogeology. Commonly, equivalence is calculated via stochastic [*de Marsily*, 1986; *de Marsily et al*., 2005; *Mariethoz et al*., 2010; *Noetinger et al*., 2005; *Renard*, 2007; *Strebelle*, 2002], heuristic [*Cardwell and Parsons*, 1945; *Dagan*, 1989; *Fleckenstein and Fogg*, 2008; *Matheron*, 1967; *Wiener*, 1912], or deterministic methods [*Chen et al*., 2003; *Fleckenstein and Fogg*, 2008; *Wen et al*., 2003; *Wen et al*., 2006].

1.3. Geophysical Methods Applied to Aquifer Numerical Modeling

Geophysical methods are proven to provide highly relevant quantitative information for investigating groundwater reservoirs [*Kirsch*, 2006; *Rubin and Hubbard*, 2005] detailing invaluable data for groundwater modeling approaches, especially in a deterministic sense. The most common use for numerical groundwater modeling is the ground application (typically cm to 10s m) of electrical and electromagnetic (EM) methods to calibrate aquifer properties, groundwater recharge/evaporation, or borehole pumping rates [*Bates and Robinson*, 2000; *Comte and Banton*, 2007; *Comte et al*., 2010; *Gedeon et al*., 2012; *Herckenrath et al*., 2013; *Sandberg et al*., 2002; *Siemon et al*., 2011].

Ground techniques are compatible with airborne conditions allowing for much larger (100s m to 1000s m) regional hydrostructural investigations related to aquifer thickness, aquifer heterogeneity, water table/water quality mapping, and large-scale structural lineaments [*Andersen et al*., 2013; *Brunner et al*., 2007; *Friedel et al*., 2012; *Gondwe et al*., 2010; *Mabey*, 1974; *Okazaki et al*., 2011; *Rasmussen et al*., 2013; *Robinson et al*., 2008; *Siemon et al*., 2011]. *Brunner et al*. [2007] in particular provide several case studies showcasing the outcomes of linking airborne geophysics (magnetics and radiometrics) and remote sensing with numerical groundwater flow models including the identification of faults and dykes.

1.4. Volcanic Dykes and Groundwater Flow Modeling

In addition to geophysics, there is an extensive log of research that indicates how to discover and assess lineaments/heterogeneity throughout a region [*Brunner et al*., 2007; *Koch and Mather*, 1997; *Nyborg et al*., 2007; *Sander*, 2007; *Solomon and Quiel*, 2006] however the integrated application with regional groundwater modeling is scarce in relation to the effects of dykes. Two studies that show regional modeling of dykes within groundwater flow models are *Morel and Wikramaratna* [1982] and *Babiker and Gudmundsson* [2004]. *Morel and Wikramaratna* [1982] combine a reduced transmissivity effect and weighted harmonic mean to account for dyke properties in a Finite Element (FE) mesh. The effect of the dykes is evidentially seen in flow simulations. *Babiker and Gudmundsson* [2004] identify that when faults (high permeability) and dykes (low permeability) intersect, they have a strong regional flow effect. There are limited studies regarding incorporating multiscale passive magnetic data into numerical groundwater flow models and no studies were found that combined multiscale geophysics, upscaling, and numerical groundwater flow modeling. This is an important portion of research to be undertaken.

1.5. Approach

In the following sections, a methodology is proposed which accounts for field scale observed heterogeneity in a regional context using a combination of both ground and airborne geophysics, upscaling techniques, and groundwater flow modeling. The Lagan Valley in Northern Ireland is presented as the study area; a relatively homogeneous, poorly consolidated aquifer that is intruded by a network of low permeability volcanic dykes. Airborne magnetics data, aerial imagery, and field-scale permeability measurements were used for this analysis (section 3). The procurement of this data provides relatable multiscale information. The methodology presented here starts with the acquisition of K values for the dyke and host rock from field permeability measurements (section 3.3). These values are upscaled to provide equivalent values for the geological units at different scales of interest (section 4). This is possible by using the analytical model of Cardwell and Parsons [*Cardwell and Parsons*, 1945] when analyzing flow parallel and perpendicular to trending dyke direction, respectively. Resulting equivalence values are incorporated into a density function to provide regional K values (section 4.1.3). The density function relies on correlating the density of outcropping dyke within a regionally observed heterogeneity against magnetic signature value. The upscaled K is

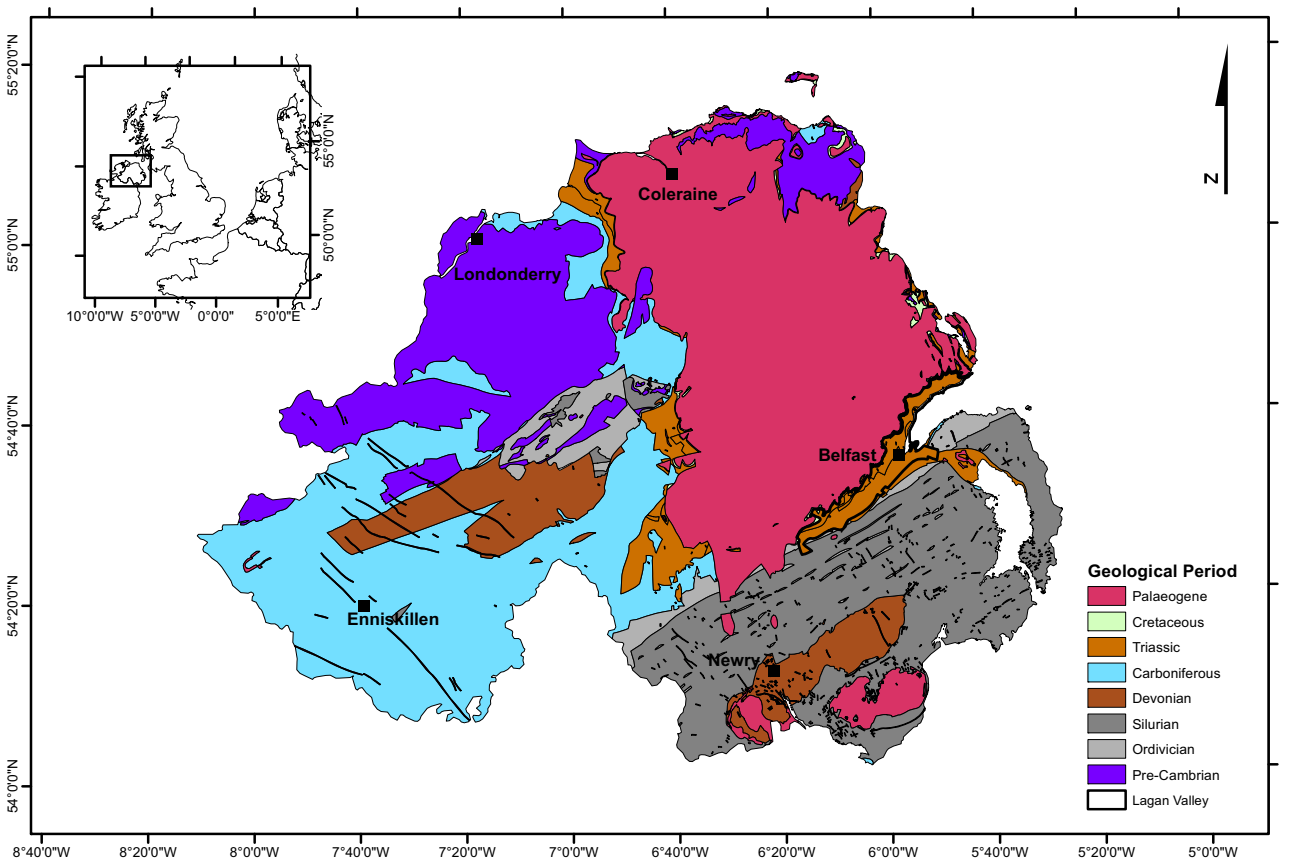

Figure 1. A simplified geological map of Northern Ireland with the Country shown in the context of Europe.

lastly used as an input for several groundwater flow models (section 5) accounting for different degrees of upscaling. Groundwater models are ultimately assessed against groundwater measurements in order to identify the method that produces results closest to the observations.

2. Hydrogeological Setting

The Lagan Valley (Figure 1) hosts an aquifer composed of Permo-Triassic sandstones, namely the Sherwood Sandstone Group (SSG), whose thickness varies from 30 to 648 m across Northern Ireland but locally, in the Lagan Valley basin reaches 300 m [*Mitchell*, 2004]. The SSG gently dips with what is thought to be approximately uniform thickness, to the northwest toward the center of the country. The aquifer is underlain by low permeability Silurian metamorphic rocks, considered as impervious substratum, which outcrop along its South Eastern border. It is overlain by a succession of low productivity marine sedimentary and volcanic rocks, aged late Triassic to Palaeogene outcropping north of the area (Antrim Plateau). The Quaternary glaciations have shaped the valley [*McCabe*, 2008] and subsequent ice melting deposited glacial till material mainly composed of clay, which constitutes a confining cover for the aquifer. The SSG is a principal aquifer for the country with overall moderate productivity. It has been studied for many decades [*Bennett*, 1976; *Cronin et al.*, 2000, 2005; *Hartley*, 1935; *Kalin and Roberts*, 1997; *Manning et al.*, 1970; *McNeill et al.*, 2000; *Robins*, 1996; *Yang et al.*, 2004] and it is well documented that the area has a large number of Tertiary doleritic dykes. These intruded during the Palaeogene period, constituting the feeding hypovolcanic network of the overlying Antrim lava flows plateau [*Cooper et al.*, 2012], now eroded in the valley. Despite the numerous hydrogeological studies undertaken, there have been no attempts to quantify the regional effect of these dykes.

The hydraulic properties of the SSG display typical K, values of 4.6×10^{-6} m s^{-1} [*Bennett*, 1976; *Kalin and Roberts*, 1997] to 9.2×10^{-6} to 4.6×10^{-5} m s^{-1} [*Robins*, 1996]. Typical transmissivity is around 1.5×10^{-3} m^2 s^{-1} and storativity of 2×10^{-3} [*Bennett*, 1976; *Kalin and Roberts*, 1997; *McNeill et al.*, 2000] and porosity is approximately 0.1–0.2 [*McKinley et al.*, 2001; *Robins*, 1996]. In addition, hydraulic tests were carried out at

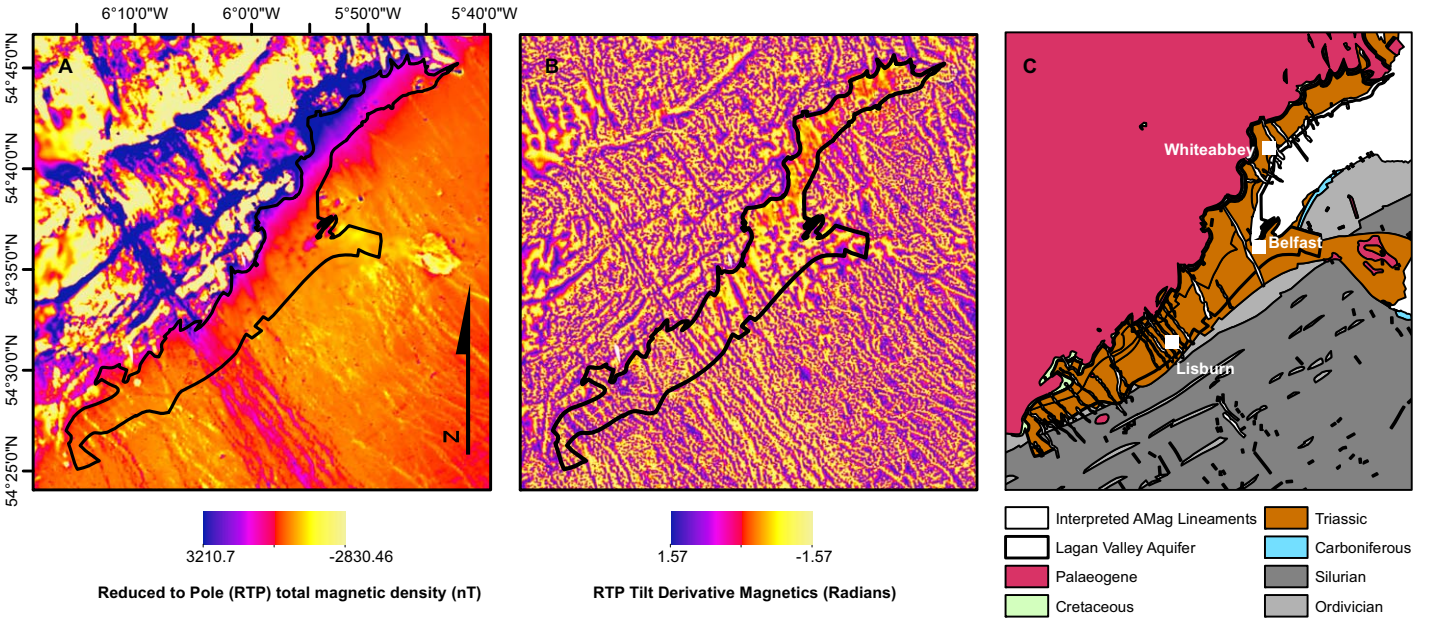

Figure 2. Images showing (a) reduced to pole (RTP) total magnetic density (nT); (b) tilt derivative of RTP aerial magnetics (radians) and; (c) digitized AMag dykes across the Lagan Valley. Important locations are labeled. Data made available by GSNI, © Crown copyright.

a study site which estimated a typical relative *K* difference of two orders of magnitude between the sandstones and dykes; 4.6×10^{-7} m s^{-1} and 8.1×10^{-9} m s^{-1}, respectively [*Comte et al.*, 2012].

3. Multiscale Observations

3.1. Airborne Geophysics

In 2005 and 2006, the British Geological Survey (BGS) and Geological Survey of Northern Ireland (GSNI) undertook an extensive airborne geophysical survey of the entire Northern Ireland, within the TELLUS project [*Chacksfield*, 2010; *Cooper et al.*, 2012]. Airborne survey lines were spaced 200 m apart and orientated NNW to ESE (165 and 345°) over the extent of Northern Ireland collecting magnetic field, electrical conductivity, and terrestrial gamma-radiation measurements. The aerial magnetics (AMag) are of interest for this study as this information can help map deep geological structures based on characteristic values obtained from variations in the earth's magnetic field [*Robinson et al.*, 2008] such as volcanic dykes and faults [*Grauch et al.*, 2001]. Reduced to Pole (RTP) and RTP tilt derivative magnetic data sets with cell size of 35 m were used (Figures 2a and 2b). The RTP data set is useful as it minimizes polarity effects from an angled placement of a dyke where there is a peak and trough of signal, normalizing the peaks directly over the source. The derivative is useful for mapping shallow basement structure [*Verduzco et al.*, 2004] however higher orders of derivatives tend to be "noisy" [*Ansari and Alamdar*, 2009] and therefore care should be taken regarding subtle anomalies when mapping features.

The AMag was digitized to obtain typical trend and width for the volcanic dykes throughout the region (Figure 2c). This was accomplished by extracting areas of contrasting higher or lower elongated magnetic anomalies, corresponding to dykes emplaced at geological periods of either normal or reverse polarity, respectively. The interpretation of dyke locations from AMag was undertaken independently from existing interpretations [*Burns et al.*, 2010; *Chacksfield*, 2010; *Cooper et al.*, 2012; *Hartmann and McConvey*, 2007] which all present variations in their account of geometry, orientation, and continuity due to different aspects being analyzed. The interpretation created here was later compared to *Cooper et al.* [2012] which constitutes the most advanced geologically based interpretation to date and a close match was found.

3.2. Ground Observations

Field investigations were carried out locally to ground proof the interpretation of the AMag; the study site (Whiteabbey) is shown in Figure 3. In the coastal study area, the dykes outcrop in the tidal flat and are

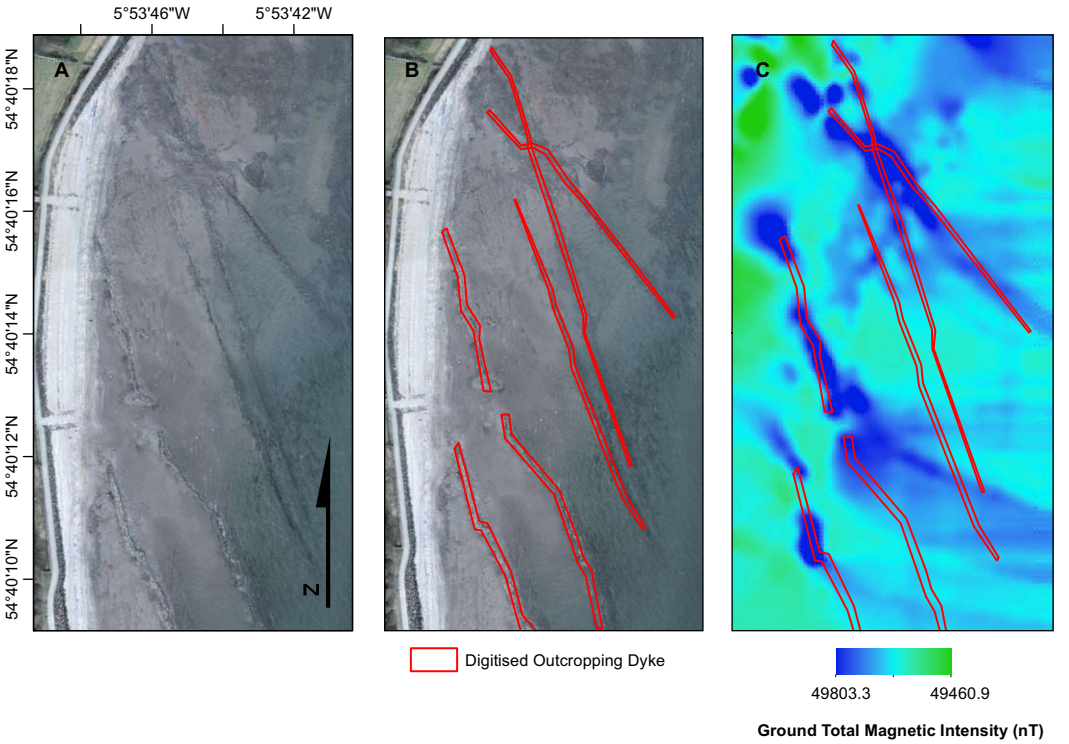

Figure 3. Locational map to show (a) georeferenced aerial imagery of study site (Whiteabbey); (b) digitized dykes observed from aerial imagery; (C) Results of ground magnetic survey across outcropping dykes. Image shows total magnetic intensity (TMI) in nanotesla (nT) © Aerial imagery Google 2013.

clearly observable on publically available aerial photos. The dykes were digitized (Figure 3b) in the same manner as the AMag and verified during site visits.

Direct observations were completed by ground geophysical surveys both in the tidal zone and in a number of fields inland, applying a passive magnetometer (GMag). The contrast observed as abnormally high measurements within the relatively constant local geomagnetic field are magnetic anomalies, e.g., dykes (Figure 3c). The combined interpretation of GMag and parallel electrical resistivity tomography (ERT) surveys [*Burns et al*., 2010] have shown that the saltwater distribution is strongly affected by the presence of the dykes, which locally confirm that they act as a relative barrier to the saltwater [*Wilson*, 2011]. Analysis of AMag RTP data and forward modeling of GMag anomalies has also suggested that dykes are deep and near vertical (dipping higher than 60° from horizontal).

The digitized locations of GMag and AMag were compared to ensure structural consistency between scales. It was found that due to the coarse nature of the AMag data, the magnetic signatures created by the several dykes at the field site are merged to create one signature at the regional scale. Other sources confirm this overlap [*Fay et al*., 2010], as was also confirmed by M. R. Cooper (personal communication, 2013). Therefore, the properties of the field site are assumed to be equivalent to one AMag heterogeneity observed at regional scale (Figure 4).

3.3. High-Resolution Permeability Measurements on Outcrops

To confirm the accuracy of literature values regarding *K* ratio and intrinsic anisotropy of dyke and sandstone, high-resolution permeability measurements were carried out. A CoreLab Portable Air Probe Permeameter—250 (PPP), was applied. The technique is suitable for obtaining intrinsic permeability in the laboratory and field locations, preferably on a flat and dry surface [*Sharp et al*., 1994]. Field permeameters have been used in various other sandstone environment studies [*Chandler et al*., 1989; *Davis and Philips*, 1990; *Fu et al*., 1994]. By injecting compressed air into a geological unit, data are determined by the unsteady state method; pressure decay is measured as a function of time, computing the intrinsic permeability (k in m^2). *K* is an intrinsic aquifer property in such that it does not depend on the fluid moving

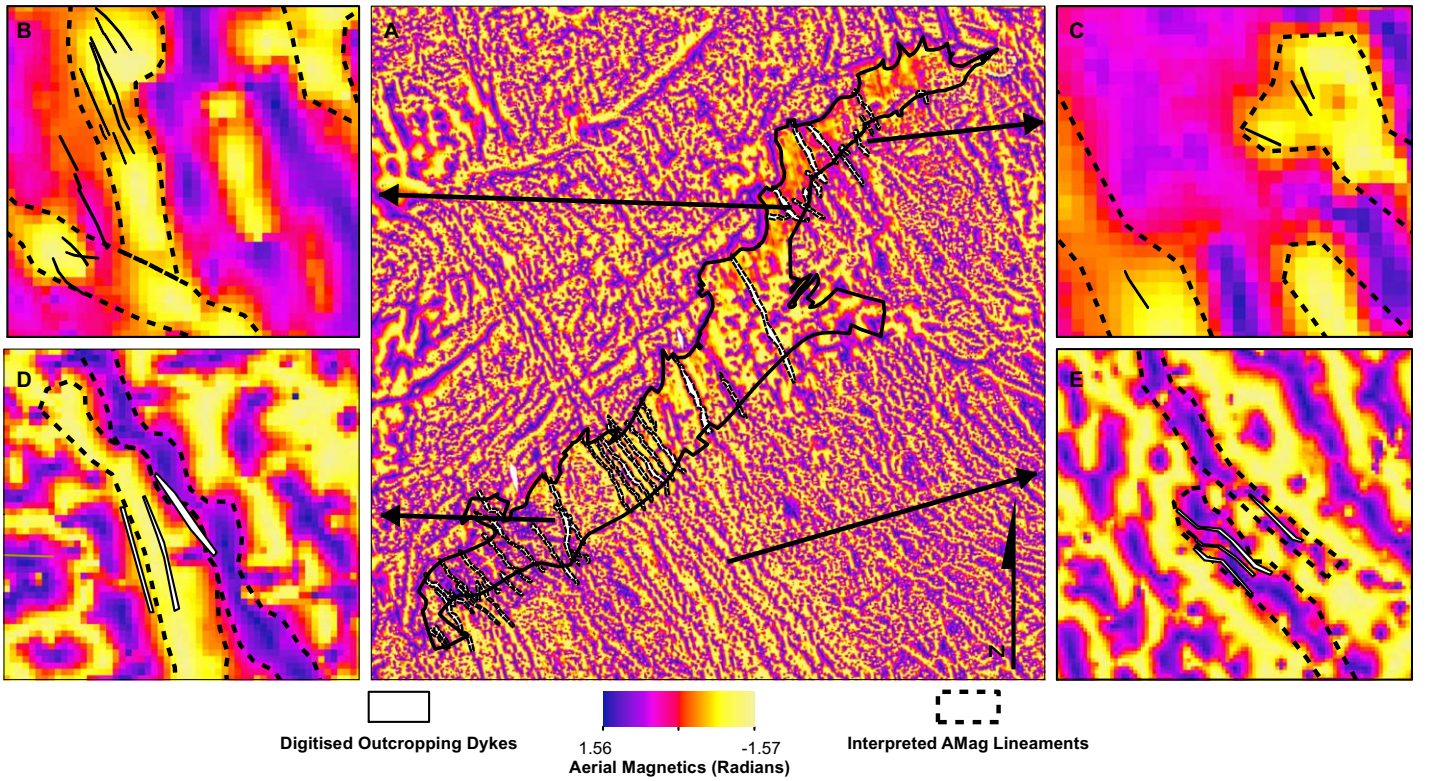

Figure 4. Image depicting AMag and GMag overlays throughout the region. Approximate AMag locations are shown by the black dashed line, aerial digitized dykes are in solid black while the expected extension of ground dykes are shown by the dotted black line.

through the pore space. The K (m s^{-1}), i.e., the permeability of water, is then obtained by applying equation (1) [*Price*, 1996; *Schwartz and Zhang*, 2003];

$$K = \frac{k(\rho g)}{\mu} \tag{1}$$

where k = intrinsic permeability, m^2; K = hydraulic conductivity, m s^{-1}; μ = absolute/dynamic viscosity of water, kg $(m\ s)^{-1}$; ρ = density of water, kg m^{-3}; g = acceleration due to gravity, m s^{-2}.

Values of μ, ρ, and g are assumed constants for freshwater and are given by, e.g., *Wilson* [1990]. Several profiles with different orientation with regard to the dyke trends were undertaken; three on site at low tide and three on blocks extracted from the site which were cleaned and allowed to partially dry. Measurements were taken across all portions of the dyke and a geometric mean taken for the dyke, dyke fractures, and sandstone to give a representative value for each field geological component. The dyke contact diagenesis (alteration of the sandstone along the plane of intrusion due to lava heat) was not classified as a different formation as in a local study, diagenesis was shown to have minimal impact on permeability beside the intrusion [*McKinley et al*., 2001] and therefore its permeability is still close to the SSG. It must be noted that this technique is perhaps not fully effective in the current conditions due to most of the surface being wet, uneven and covered in mud/crustaceans. This led to a true seal not being possible for many of the values which could then not be included. A true seal refers to placing of the PPP nozzle onto an ideally flat rock surface. If the nozzle is not placed firmly onto the rock surface, when implemented, compressed air can easily escape from the chamber and does not penetrate into the rock. For this work, the absolute values are not required. Instead, the relative values between the dyke and sandstone allow confirmation of the permeability ratio obtained from the complementary hydraulic investigations. Fracture widths were measured using a feeler gauge accompanied by a compass bearing and picture.

After calibration of the PPP to the sandstone, where K has been locally measured by hydraulic testing at 4.6×10^{-7} m s^{-1} [*Wilson*, 2011], it was concluded that the K of the sandstone, dyke matrix, and dyke fractures

Table 1. A Summary of Literature and Research Values for *K* Throughout the Lagan Valley

Geological Unit	*K* From Hydraulic Testing (m s^{-1})	*K* From Numerical Modeling (m s^{-1})	*K* From PPP (m s^{-1})
Sandstone			
Main regional aquifer	4.6×10^{-6} to 4.6×10^{-5}[a]	2.3×10^{-7} to 5.27×10^{-5}[b]	n.a.
Whiteabbey site	4.6×10^{-7}[c]	4.6×10^{-7}[c]	7.6×10^{-7}[d]
Dolerite Dyke (Whiteabbey Site)			
Dyke bulk	n.a.	2.0×10^{-8}[c]	n.a.
Dyke matrix	n.a.	n.a.	4.4×10^{-9}[d]
Dyke fracture	n.a.	n.a.	1.2×10^{-7}[d]

[a] *Bennett* [1976], *Kalin and Roberts* [1997], and *Robins* [1996].
[b] *Cronin* [2000].
[c] *Wilson* [2011].
[d] This study.

were equal to 7.6×10^{-7}, 4.4×10^{-9}, and 1.2×10^{-7} m s^{-1}, respectively (Table 1). A lack of perfect match between *K* from hydraulic testing and *K* from PPP can be attributed to discrepancies in the rock surface. Values from hydraulic tests on boreholes, i.e., pumping tests in this case, are representative of a deeper and much larger volume of aquifer, in comparison to the PPP tests. PPP only measures the weathered and clay washed surface, therefore producing higher permeability values. Relatively, both hydraulic and PPP measurements suggest two orders of magnitude difference between sandstone and dyke *K* at the Whiteabbey site. At regional scale, assuming that the *K* of the dykes does not vary significantly, the *K* difference between the sandstone (regionally established average value of ~1 m $d^{-1} = 1.2 \times 10^{-5}$ m s^{-1}) and dyke would then be around three orders of magnitude. At Whiteabbey, the sandstone *K* is approximately 10 times lower than the value of the main regional aquifer due to its location in the upper part of the Permo-Triassic, which corresponds to a transition facies with the overlying lower permeability Mercia Mudstone.

4. Upscaling of Hydraulic Conductivities

4.1. Upscaling Technique

4.1.1. Principle

An upscaling technique is applied, which is the result of a conjunctive analysis of petrophysical and geophysical components, creating a deterministic solution of heterogeneities at different scales. It is an analytical solution of the diffusion equation as detailed in *Renard and de Marsily* [1997] and *Renard et al*. [2000]. The dyke's inherent heterogeneities (i.e., fractures and fissures) are accounted for while the sandstone is assumed to be homogeneous. The region can be observed as a hierarchical system [*Klingbeil et al*., 1999] were the heterogeneity at each observation scale is defined through equivalence and anisotropy calculated from the previous scale (Figure 5). The heterogeneities are concluded to be vertical cuboids of uniform thickness, emplaced in a unit of host rock, as confirmed by GMag modeling [*Comte et al*., 2012].

We assume in this work for simplicity that AMag anomalies are composed of a number of parallel vertical dykes (Figures 4 and 5). We therefore apply the upscaling model defined for banded formations by *Cardwell and Parsons* [1945]. At each level, equivalent *K* within a heterogeneous block is calculated, where if flow proceeds parallel to the heterogeneity it is characterized as the arithmetic mean (μ_a) and when perpendicular, the harmonic mean (μ_h) [*Cardwell and Parsons*, 1945]. At each upscaled level the anisotropy ratio also is calculated (μ_a/μ_h), using the equivalent *K* obtained from the previous lower-scale level. Therefore, at the largest regional scale each heterogeneity has the equivalent *K* and associated anisotropy created from field-scale geological observation, which are also summarized by equivalent *K* and associated anisotropy of permeability from outcrop measurements. The calculations used are expressed by the following general equations:

Hydraulic conductivity parallel to heterogeneity planes:

$$K_{\parallel} = \mu_a = \frac{\sum K_i \cdot d_i}{\sum d_i} \tag{2}$$

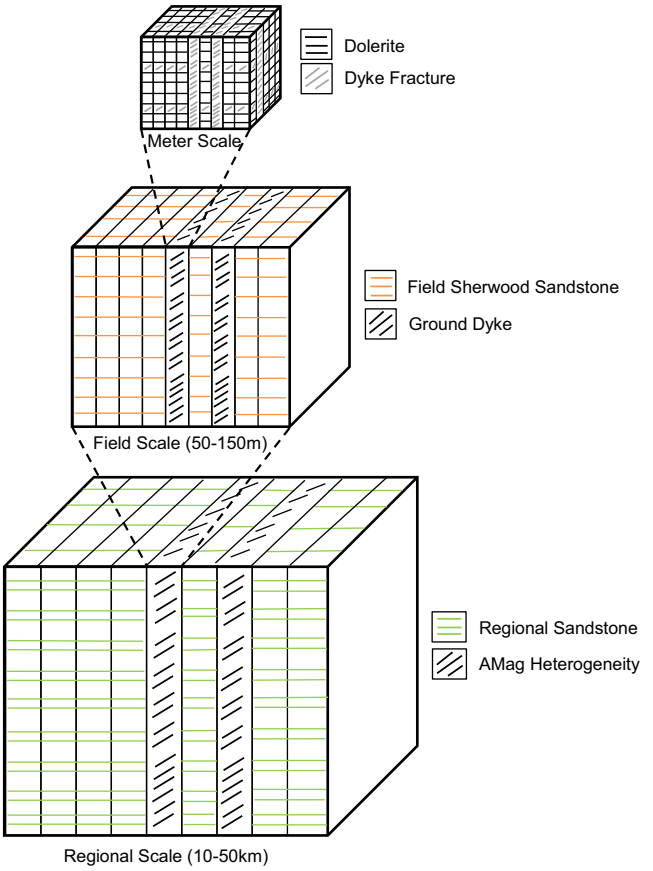

Figure 5. Diagram showing the relation of equivalent blocks and upscaling in a hierarchy system

Hydraulic conductivity perpendicular to heterogeneities planes:

$$K_{\perp} = \mu_h = \frac{\sum d_i}{\sum \frac{d_i}{K_i}} \quad (3)$$

Anisotropy ratio:

$$\alpha = \frac{K_{\parallel}}{K_{\perp}} \quad (4)$$

where $K_{\parallel}$ = equivalent parallel hydraulic conductivity (m s^{-1}), $K_{\perp}$ = equivalent perpendicular hydraulic conductivity (m s^{-1}); K_i = hydraulic conductivity of vertical sheet (fracture and dyke matrix at the outcrop scale; GMag dyke and host sandstone at the field scale; AMag dyke and host sandstone at the region scale; AMag cluster at higher scale; etc.) (m s^{-1}); d_i = width of vertical sheet (m); α = equivalent anisotropy ratio (–).

This technique requires a conceptual idea of geological structure as determined from visual analysis to which values will be upscaled, i.e., the total width, angle and characteristic *K* of both the block matrix and the local heterogeneities, independently.

4.1.2. Outcrop-Scale (mm to m)

At the initial outcrop-scale (mm to m), permeability measurements are taken for both the dyke fractures (local heterogeneities) and the unfractured matrix (host rock). Using μ_a and μ_h applied to selected transects perpendicular to fracture orientations (two main orthogonal trends are observed, parallel and perpendicular to the dyke trends) an equivalent *K* is created for the block (i.e., the fractured dyke) in the parallel and perpendicular directions to the dyke trend, respectively.

As the fracture density increases, so does the anisotropy ratio due to dispersion in $K_{\parallel}$ and $K_{\perp}$ values. The perpendicular value is remaining relatively stationary while the parallel value increases marginally. However, this increase is not significant. It would appear that the fractures are not influential enough to create any effect across the section of the dyke, creating a medium that is relatively homogeneous. Therefore, the dykes are treated as isotropic with the resulting $K_{\parallel}$ and $K_{\perp}$ being almost equal. As a result, the geometric mean of the dyke (5×10^{-9} m s^{-1}) is used as an initial value in subsequent upscaled blocks. This value is approximately 100 times lower than the sandstones calculated from hydraulic tests by *Wilson* [2011] at Whiteabbey.

4.1.3. Field Scale (m to 100 m)

At the field scale (m to 100 m), the equivalent dykes are considered as the heterogeneities and the sandstone as the host rock. The calculations of μ_a and μ_h are again used but based on dyke density as calculated from the magnetics. To make this possible, a correlation was established between the dyke density and strength of the AMag signal. This was founded on all visible outcrops within the region (13 sites) and produced a correlation that was strong ($r^2 = 0.9518$) as seen from Figure 6. The equation of the line was then rearranged to obtain the dyke density throughout the region as a function of the AMag. However, due to urbanized locations and mixture of geology throughout the region, the magnetic signal is not clean and therefore contains "noise." This was structurally processed before use in the groundwater model. As a result of this processing, the calculated dyke density based on lineament AMag magnitude was applied where clear lineaments were observed and

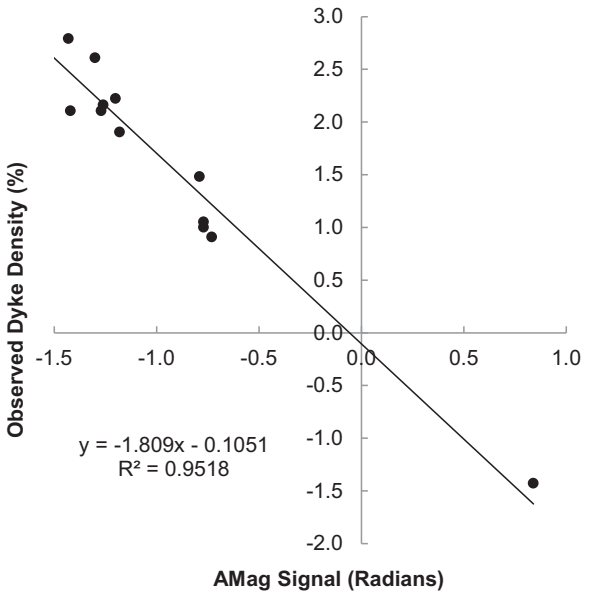

Figure 6. Graph showing the correlation between observed dyke outcrops throughout the region and their associated magnetic signal as derived from the tilt derivative data. Positive and negative densities reflect normal and reversed polarity observations, respectively.

digitized (section 3.1 and Figure 2c). Outside those clear lineaments, attributed to dyke occurrences, a density of zero was applied.

This density map was subsequently used to calculate $K_{\parallel}$ and $K_{\perp}$ across the region using equations (2) and (3). Theoretical regional variations of K values, using the observed and probable range of dyke density are plotted in Figure 8. Within this model, the mean regional K value for the host sandstone was used as it is well documented to be 1.2×10^{-5} m s^{-1}. The study site is local and not representative of the whole region as discussed above. Figure 7 shows that $K_{\perp}$ rapidly decreases up to nearly three orders of magnitude with increased dyke density (Figure 7a). It also shows that $K_{\parallel}$ does not vary significantly with dyke density. Overall, this results in an increase in anisotropy illustrated by $\alpha = K_{\parallel}/K_{\perp}$ (Figure 7b). The K distribution derived from the dyke density distribution itself derived from AMag data is directly input to the groundwater flow model. Due to the resolution of the AMag, the dispersion of K across the magnetic lineaments in the perpendicular direction was quite coarse and in places, disjointed. It was therefore deemed appropriate to assign the most extreme K value within model elements, i.e., if internal $K_{\perp}$ varies between 2×10^{-9} and 2.6×10^{-8}, then 2×10^{-9} was assigned to the entire digitized lineament. Both the direct correlation and extreme value scenarios are simulated.

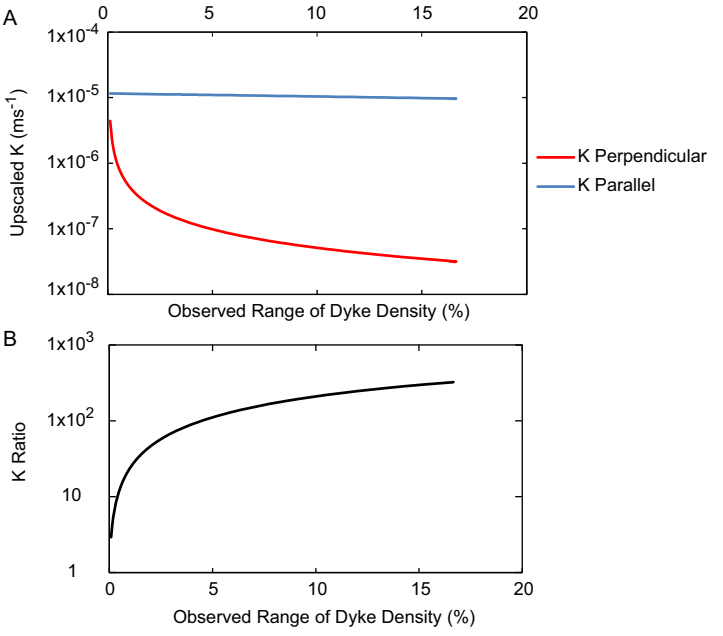

Figure 7. Graphs indicating; (a) *Cardwell and Parsons* [1945] analytical solutions of the equivalent parallel K (arithmetic mean, blue line) and perpendicular K (harmonic mean, red line); (b) increase of K ratio with increased dyke density.

4.1.4. Subregion and Region-Scales (100 m to 10 km; 10 to 100 km, Respectively)

We upscale further to summarize the many trending dykes across the valley. The area was split into further zones, as dictated by clustering or similarly orientated groups, and analyzed once more by μ_a and μ_h. This makes the region one large block made of 12 smaller blocks. This is providing a coarse representation of the anisotropy across the region.

4.2. Interpretation and Sensitivity

A summary of scale effect on anisotropy is shown in Figure 8 by presenting the possible anisotropy ratios that could be observed at each upscaled level.

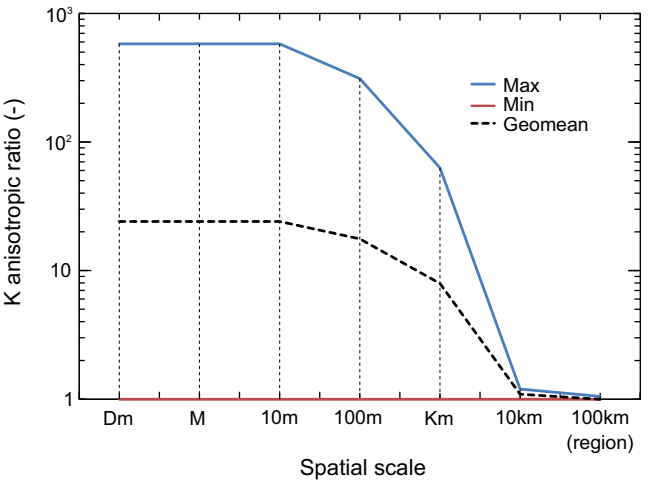

Figure 8. Graph showing the maximum and minimum anisotropy value theoretically possible at different upscaling levels.

The graph demonstrates that with an increase in upscaling, anisotropy decreases as the effect of the dykes is lost amidst the dominant sandstone. For modeling, the 100 m scale has been chosen as the minimal upscaling level as it retains a large portion of the anisotropy effect without the computational burden and infeasibility of a meter scale gridding. Choosing this minimum level of modeling would generally be accepted due to the compromise between complexity and computational burden, but higher degrees of upscaling are also investigated in this work.

5. Numerical Groundwater Flow Modeling

Groundwater modeling has been undertaken using the Finite Element Method (FEM) available within FEFLOW 6.1 (DHI-WASY GmbH). The physical structure was imported from geological shapefiles of the SSG from the GSNI. No flow boundaries were assigned to the majority of the North and West as well as the South (basement outcrop). The East boundary is connected to the Irish Sea (Belfast Lough) and was assigned a constant head corresponding to the mean sea level. A groundwater divide was mentioned in literature to the South-East corridor of the aquifer [*Bennett*, 1976] and was observed in initial groundwater simulations. This boundary was therefore shortened and instead an entering flux equal to the corresponding recharge between the domain boundary and the water divide was determined. The recharge of the aquifer was assigned as a function of outcropping geological unit: Sherwood Sandstone ranges from 73 to 100 mm yr^{-1}; below the Mercia Mudstone 7–10 mm yr^{-1} and below the Basalt 4 mm yr^{-1}. Ranges were implemented to account for urbanization, *K* of overlying geology and glacial till cover, all of which may decrease potential recharge. Values used remain within literature estimations [*Cronin*, 2000; *Kalin and Roberts*, 1997; *Manning et al*., 1970]. Topography was created using elevation data points recorded at 5 m intervals. The Lagan River was simulated by providing initial head values extracted from the digital elevation model (DEM) and a spatially varying constant head (called fluid transfer or Cauchy boundary condition in FEFLOW) was assigned to the adjoining nodes and element sides. The river bed conductance varied along the length of the river to account for till and a consequential reduction of connectivity due to a thick clogging layer. This was split into three sections: upper and lower Lagan [*Cronin*, 2000] plus the area overlapping with the Mercia mudstone. Finally, the pumping rates were input as constant point fluxes (outputs). The river elevation was extracted from the Ordnance Survey of Northern Ireland (OSNI) elevation data while the conductance was altered depending on the observed till thickness. Groundwater abstraction rates were extracted from previous work [*Cronin*, 2000] and updated alongside points received from the Northern Ireland Environment Agency (NIEA) (personal communication, 2013). The points are still limited and it is thought that all current abstraction rates are not accounted for here, mainly in the city due to changing commercial needs.

As indicated in section 4.1, there were five simulations run: (#1) isotropic model, (#2 and #3) field-scale anisotropy from two scenarios of field-scale upscaling, (#4) subregional anisotropy, and (#5) a single anisotropic value model. A summary is given in Table 2. The inputs were the equivalent *K* data perpendicular (in plane (X, Y)) and parallel (in both plane (X, Y) and direction (Z)) to dyke trends with each model containing varying angles of anisotropy (Figure 9). For comparison, Figure 10 includes an interpolated surface of 124 observed static water levels: a composite data set of values from the literature, previous models and borehole records spanning from 1935 to 2011. The head data points were interpolated using Inverse Distance Weighting (IDW) with eight neighbors and cell size of 100 m. This provides a visual frame of reference to analyze modeling results.

Table 2. A Summary of Different Models Run and a General Description of Input[a]

Model Number	Model Description	Model Input	Anisotropy Angle	Parameters Simulated
(#1)	Isotropic	Base value of 1.2×10^{-5} m s^{-1} applied in all directions	0°	3
(#2)	AMag anisotropic	Anisotropy applied across whole region as a direction function of equivalent *K* correlated from AMag signal	Different value added to each dyke: range of 2–87°	3
(#3)	Single anisotropic	A single equivalent *K* given to each dyke based on the maximum positive or negative value	Different value added to each dyke: range of 2–87°	3
(#4)	Subregion	A total of 13 anisotropy values and angles applied based on an equivalence generated by grouping similar clusters of dykes	One value per subregion: 25–87°	3
(#5)	Regional	One anisotropy value based on an equivalence created for the entire region	One value of 31°	3

[a]Parameters simulated are $K_{||}$, $K_{\perp}$, and θ which vary for each model as a result of upscaling technique.

The different flow simulations were further verified quantitatively through comparison of resulting correlation coefficients (r^2), root-mean-square errors (RMSE) and model ranking via Akaike's Information Criterion (AIC). Calculation of r^2 and RMSE are commonly used for evaluating the accuracy of deterministic predictions [*Duan et al*., 2007]. When calculating regression, the best fit is when simulated hydraulic heads are equal to observed heads, i.e., y = x, producing a slope *m*, of 1 through the origin, (0,0). Calculating the associated sum of the squared residuals [$\sum(y - \hat{y})^2$] provides data for r^2 and RMSE.

AIC [*Akaike*, 1973; *Carrera and Neuman*, 1986; *Burnham and Anderson*, 2002] provides a measure of relative estimations of uncertainty to help determine a balance between model complexity and improved model regression. A key property of AIC analysis is the penalty associated with over parameterization of models. An increase in parameters increases the final AIC value, suggesting a more unreliable simulation, as the model with AIC closer to zero is the optimum. An extended criteria, AICc, should be used when sample size is small ($n \div N < 40$, where *n* is the number of data points and *N* is the number of estimable parameters) [*Burnham and Anderson*, 2002, 2004; *Hurvich and Tsai*, 1989, 1995; *Poeter and Anderson*, 2005]. This second-order bias correction is not appropriate in this circumstance as the models contain 124 observation points and each simulates three parameters, i.e., $n \div N > 40$. The same three parameters are simulated for each model: $K_{||}$, $K_{\perp}$, and anisotropy angle θ. The application of θ alters the axis enabling K_z to equate $K_{||}$ and is dependent on the trending heterogeneity direction. Formula described in *Ye et al*. [2008] is implemented here to provide AIC and the model weights (AIC w_i). Weights are the relative likelihood of the model given the data which are normalized to sum to 1 and interpreted as probabilities. The AIC equation is defined as:

$$AIC = n \ln\left(\hat{\sigma}^2_{ML}\right) + n \ln(2\pi) + n + \ln|Q^{-1}| + 2p \tag{5}$$

where *p* is the number of model parameters plus one, *n* is the number of observations, *Q* is the weight matrix and $\hat{\sigma}^2_{ML}$ represents an estimate of the variance of weighted residuals, defined as:

$$\hat{\sigma}^2_{ML} = \frac{\sum_{j=1}^{n} (\varepsilon q)_i^2}{n} \tag{6}$$

where ε is the residuals and *q* the weight of the *i*th observation. The method is steadily being more involved with groundwater models [*Engelhardt et al*., 2013; *Foglia et al*., 2007; *Hill*, 2006; *Hill and Tiedeman*, 2007; *Parker et al*., 2010; *Poeter and Anderson*, 2005; *Singh et al*., 2010; *Ye et al*., 2010]. This allows each model to be described in terms of its results in a comparative manner.

6. Model Results and Discussion

6.1. Model Simulations

For each model, a summary of r^2, RMSE, and AIC are provided for the entire region, plus a refined upstream selection (Table 3). Many of the observation points available are close to the Irish Sea which is controlled by a constant head boundary. By separately analyzing only the points which are upstream of Belfast and where 90% of the heterogeneity exists, it may provide a more representative analysis of model fit. Additionally, a

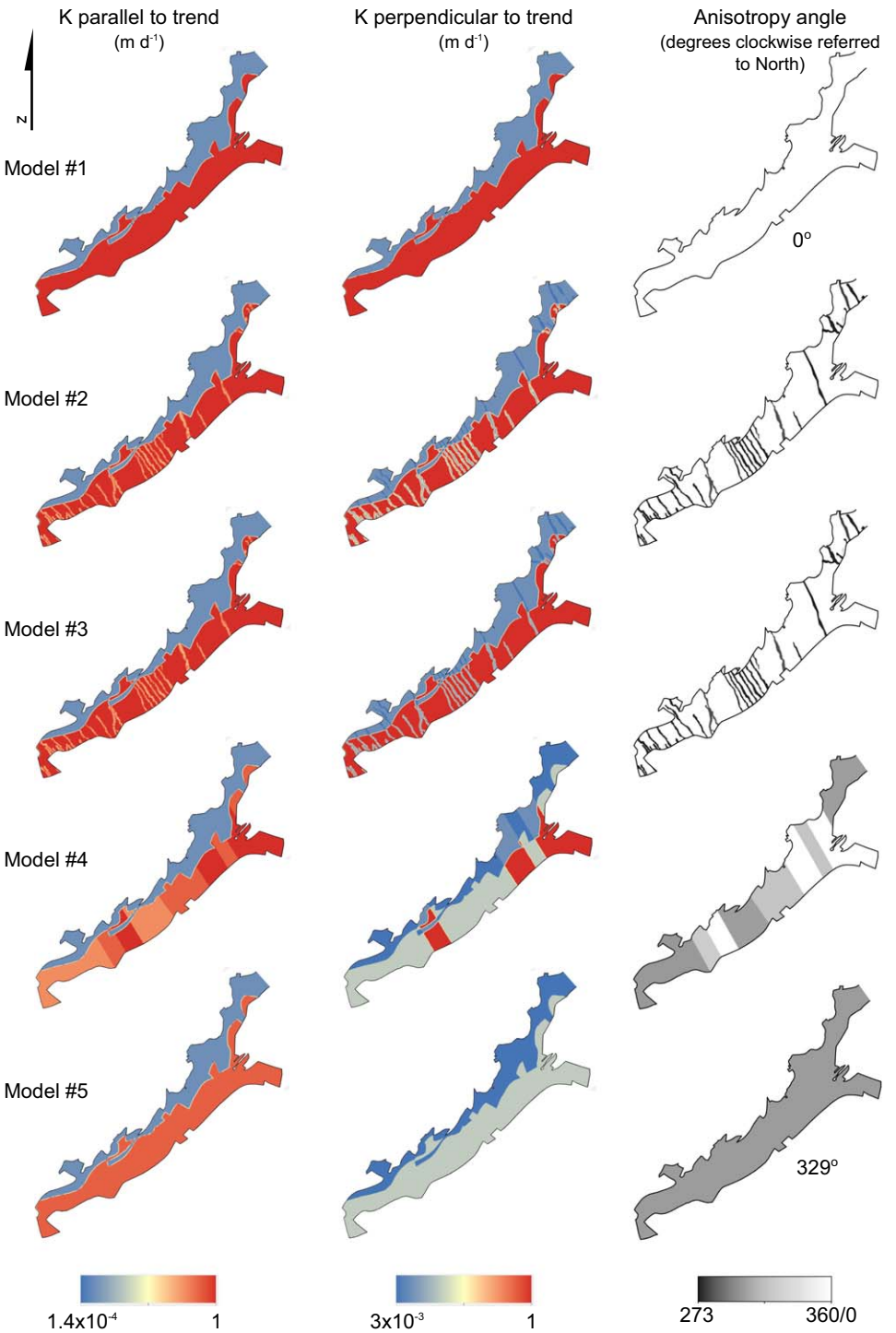

Figure 9. Maps showing model inputs for each of the five models simulated. *K* parallel and perpendicular to dyke trend are displayed alongside the anisotropy angles.

scatter plot of simulated versus observed hydraulic head values is provided alongside the simulated flow direction (as calculated from interpolated head values) and presented in Figure 10.

The initial model (#1; isotropic) generally produces a satisfactory result despite being constructed from very little data and parameters. Overall, the simulated head values are lower than the observed heads

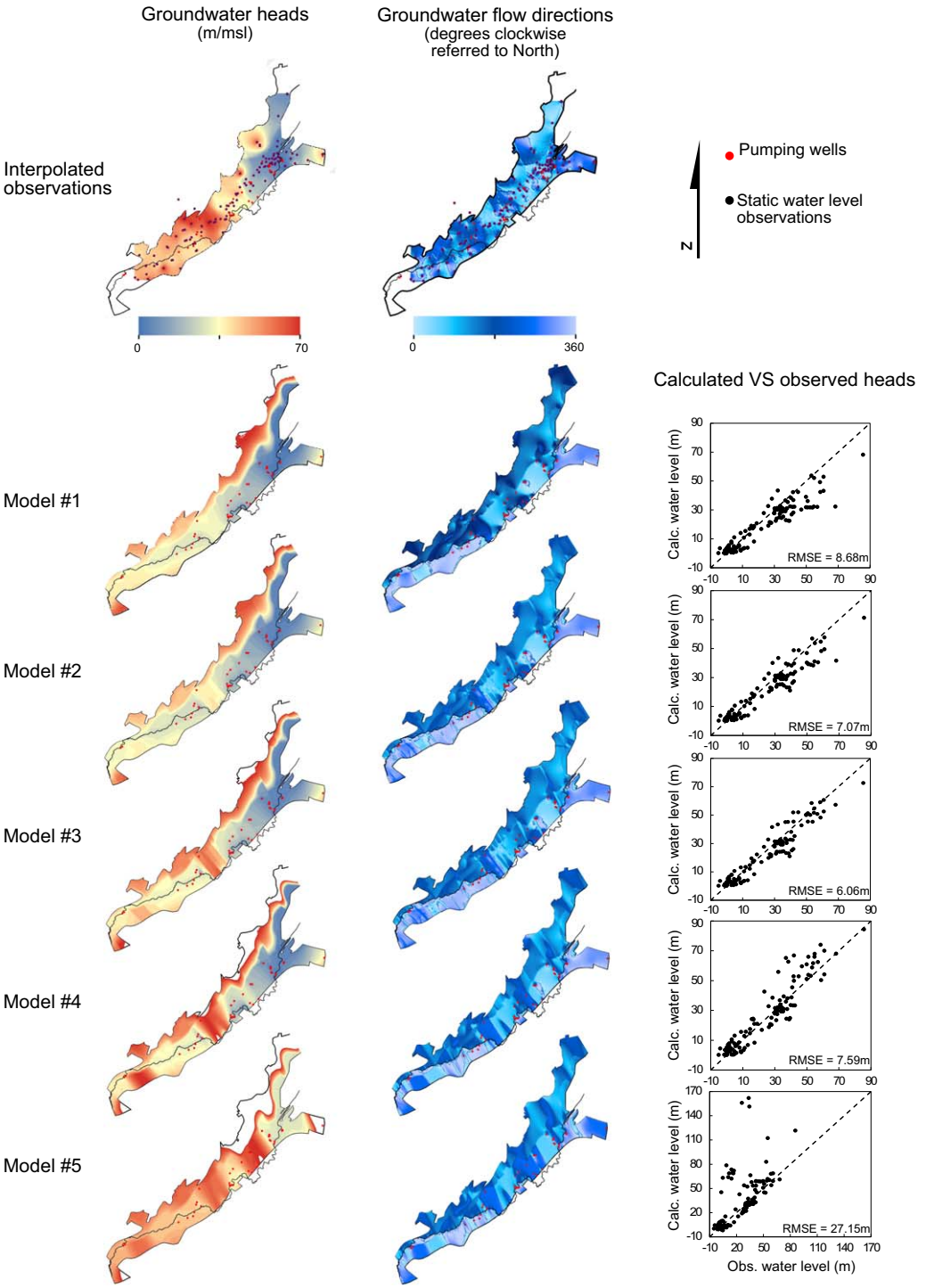

Figure 10. Maps displaying the simulated groundwater head values throughout the Lagan Valley for each of the five models accompanied by maps of simulated flow direction. A reference groundwater head and flow direction surface is created from interpolated observation points. Model regression is provided to show the fit of the models alongside the root-mean-square error values.

with most erroneous points leveling out at one particular location: the center of the region. This suggests that a component could be missing that would usually allow groundwater build up, perhaps from compartmentalization. This is the area of a dense heterogeneity band simulated in models #2 and #3. This could be an influence on the high RMSE of 8.68 m. The best areas of fit are the lower head values located at the coast, which is well constrained by the constant head boundary condition.

Table 3. A Summary of Comparative Model Statistics Including: Regression Coefficient (R^2), Root-Mean-Square Error (RMSE), Akaike's Information Criteria (AIC), and Weighted AIC (AIC w_j)[a]

Model	R^2	RMSE (m)	AIC	AIC w_j
#1	0.68/0.39[b]	8.68/10.24[b]	429/322[b]	0/0[b]
#2	0.83/0.68[b]	7.07/8.28[b]	378/286[b]	0/0[b]
#3	0.89/0.82[b]	6.06/7.03[b]	340/258[b]	1/1[b]
#4	0.88/0.83[b]	7.59/8.76[b]	396/295[b]	0/0[b]
#5	0.32/0.27[b]	27.15/31.57[b]	712/513[b]	0/0[b]

[a]Analysis suggests that model #3 is the most probable due to highest r^2, lowest RMSE, lowest AIC and probability of 1 for AIC weight.
[b]Statistics for the upstream half (SW) of the aquifer only, where 90% of lineaments occur.

Perhaps, additionally, with such a simplistic geology, the river is having too great an influence. It is thought that the river has an effect in every model due to known connectivity however in the alternative models; the AMag heterogeneities also alter flow direction, creating varying accounts of groundwater availability to the river. In this model, the region has a dominant flow direction of 59° from the North which is a generalization of the Northward and Southward flow to the river (Figure 10).

The first anisotropic model (#2) was based on the direct correlation between magnetic signal and dyke density as was detailed in section 4.1.3 (Figure 6). In this model, each AMag dyke is internally heterogeneous, with generally smooth *K* transition between elements. However, this could suggest the dyke does not act as a complete barrier. Each dyke is also assigned its own angle of anisotropy (Figure 9). The resulting correlation ($r^2 = 0.83$) is a significant improvement compared to #1. Most values are still simulated lower than observed values suggesting the internal heterogeneity and possibly contrasting element values are creating unrealistic flow; there is a potential for internal compartmentalization in the AMag lineaments. When the upstream observation points are analyzed, this models performance significantly decreases to that of an r^2 of 0.68 and a high RMSE of 8.28 m.

The second anisotropic model (#3) is similar to #2 however the dykes are internally homogeneous. Each dyke has an individual angle as before (Figure 9) but additionally an individual *K* which is the maximum observed within that dyke from #2. The resulting correlation ($r^2 = 0.89$) is the best fit of all simulations. In terms of regression and RMSE, this model is performing the best with only 6.06 m error. The dykes are allowed to act as barriers, as was observed at the field scale. The band of higher water levels correlating with the dense heterogeneity band and observed in the interpolated map is also present and generally, the points in this zone are well matched. The compartmentalization and alteration of flow direction is evidently seen in Figure 10 with the groundwater flow trending parallel to the dyke locations and perpendicular to general groundwater flow direction. Average flow direction is North East at 46° complements the conceptual model well. From AIC analysis, this model performed the best with the lowest value, and a probability of 1 using a weighted analysis, suggesting the optimum model. This effectively shows the effect of including heterogeneity.

When the region is upscaled again to be based on subregional zones (#4) and a new equivalent *K*, the values are beginning to be simulated higher than expected. This is due to an over estimated value of equivalence which is acting in long, ridged compartments. Additionally, the arithmetic and harmonic means produce extreme upscaled values, which become evident when an equivalent value is calculated for such a large region. As the upscaling is now not limited to the digitized AMag lineaments but rather the entire subregion (Figure 9), this method implies applying *K* anisotropy (and arithmetically averaged anisotropy direction) to areas where there is no lineament observed. The equivalence is therefore producing a coarse and possibly too simplistic anisotropy distribution. This has a strong effect on simulated heads (Figures 10) and is reflected in the high RMSE and relatively high AIC value.

Finally, when the region is taken as a whole (#5) the simulation is highly erroneous ($r^2 = 0.32$) with some values approximately 100 m above what is observed. This is because the model is suggesting an overestimated, extreme anisotropy value in areas where heterogeneities do not exist, creating an unrealistic flow vector regime which is effecting other areas within the region. As with #4, the applied anisotropy direction is creating an extreme additional flow component which is not necessary. Additionally, the average flow direction in this model equates to approximately 300° suggesting a North West direction opposed to the known North East direction. In this simulation, the effect of the river has been overcome due to an overestimated anisotropy.

Computationally, all models took a similar length of time to converge. Equilibrium of inflow and outflow was quickly calculated and the simulations took under 1 min to run. As a result, all models are equally feasible.

6.2. Comparison With Previous Studies

When compared to previous work undertaken by *Bennett* [1976], *Cronin* [2000], and *Hartley* [1935], who have all mapped groundwater in the region, the results presented here produce an outcome with some similarities and some distinct differences. As point locations of the static water level were extracted from these aforementioned studies and the work here is producing a simulation close to these, one could summarize that the studies are relatively similar in terms of water head response. However, due to the higher observation density used in this study, heterogeneities derived from new airborne magnetics data, particularly around the large dyke swarms (e.g., area around Lisburn) are being better represented than previous studies with a lower observation density. That is until the flow angles are observed (Figure 10). Despite static water levels (SWLs) matching, the direction of flow is distinctly different in several locations. Along the length of the river produces similar flow lines and values, suggesting that the riverbed conductance has been accurately mapped and acts as a strong control on groundwater flow in its vicinity. The area underlying the City of Belfast is also a close match with similar directional flow lines. The major differences are within the central, and SW portions of the model. From the AMag maps, the SW contains another band of dykes which the former studies do not appear to be affected by. The results presented here with an updated geological model are hydrostructurally different to those of previous works by, e.g., *Cronin* [2000], *Cronin et al*. [2000], and *McNeill et al*. [2000]. The fundamental difference with previous authors is the integration in this study of a well-constrained multiscale geological foundation. In contrast, previous authors applied arbitrary hydrogeological zonation and parameterization from inverse modeling (PEST) [*Doherty*, 1994] used to maximize the fitting of model outputs to observations.

It can therefore be stated that the results produced here are holistically different from previous studies yet produce validated statistical evidence that the method used is first; more accurate than an isotropic model and second; accounts for meter scale heterogeneity at a regional scale. In all scenarios the cluster of points with simulated heads at a maximum of 10 m above mean sea level, appear accurate and do not dramatically change between simulated scenarios. These are located in the Belfast vicinity, where dykes have not been clearly mapped and where groundwater levels are strongly controlled by the sea level boundary. If these points are excluded, a larger difference between models can be observed (Table 3). The area with most change occur upgradient around the center and the identified dense bands of lineaments. The river is a major influence and has a large impact on the direction of flow however it cannot be denied that the inclusion of dykes alters the flow directions. This can have implications for future groundwater abstraction as a new vision of groundwater flow and yield can help with sustainable management of the aquifer, ensuring progressive reduction and prevention of pollution. This could prove crucial when defining and monitoring protection zones for water wells. With the isotropic model, contributing volumes to pumped boreholes will tend to extend at the SW of the borehole while for the anisotropic model; it will tend to extend parallel to the dykes, i.e., NW or SE. With the latter model regulators are able to delineate borehole protection zones more accurately which is important for regional groundwater management and sustainability measures.

7. Conclusions and Future Work

It has been shown that by creating deterministic models of the geology based on the literature knowledge, field studies observations, and multiscale geophysical surveys, it is possible to upscale geological heterogeneity parameters yet still capture geological realism. This creates a fast and effective method for modeling regional groundwater flow based on obtained parameters from site measurements. By calculating equivalent hydraulic conductivities at several levels structurally constrained by geophysical data, the proposed method accounts for the heterogeneity within heterogeneities, creating a more robust geological conceptualization and therefore more realistic hydrogeological parameters. Evaluation is provided through the correlation of simulated and observed head levels and information criteria analysis, AIC. When the upscaling method is applied to well-defined literature parameter inputs, the anisotropic model produces an increase in correlation. Based on AIC weighting, model #3 is the best from the data presented here, complying with the r^2 and RMSE values. The consistency between piezometry statistics and

AIC mirrors the results of *Foglia et al*. [2007]. Despite a lower regression, model #2 is ranked second, most likely as a result of the lower RMSE. Unsurprisingly, model #5 is the worst as a result of over exaggerating the size of heterogeneities and attributed anisotropies. When only the upstream observation points are analyzed, the overarching result is the same, with model #3 being the optimum model. Model #4 provides a marginally better regression however a relatively higher AIC value. A joint quantitative analysis proves highly beneficial. The method presented here requires little computational burden and suggests known parameter distribution at various scales instead of computerized parameter estimation (e.g., by inverse modeling) which can sometimes provide unrealistic distributions. The model produced here has built on existing knowledge and despite a perfect correlation not being obtained, has given insight into the effect of dykes on a regional scale and improved the conceptual understanding of this region and its groundwater resources.

More research is required regarding how best to extract heterogeneities from aerial geophysics and possibly investigating if other geophysical methods are more appropriate than magnetics. Depending on the geological setting, the method can be easily applied to other airborne geophysical data, such as electromagnetics. There is also a need to test this method in alternative geological settings which will have different heterogeneity conditions and structure, e.g., higher permeability features in hardrock/basement or karstic context, in particular where structure than cannot be assumed to be "banded." Alternative AMag realizations are also needed, perhaps through utilization of stochastic methods and multiple-point statistics (MPS). This can analyze the aerial geophysics to provide many equally probabilistic alternatives of AMag distribution in order to improve the lineament computation particularly in noisy regions [*Dickson et al.*, 2014]. The deterministic and equivalent field model and parameters may continue to be used as equivalence for this new interpretation.

Acknowledgments

This work was carried out thanks to a PhD scholarship funding from the Northern Irish Department of Education and Learning. We acknowledge the Northern Ireland Environment Agency for supplying regional pumping rates and the Geological Survey of Northern Ireland for supplying Tellus airborne geophysical data, borehole records, and GIS shapefiles; in particular, Alex Donald, Mark Cooper, and William Smyth. Hugh Anderson from Midland Valley is also thanked for supplying GIS dyke shapefiles as well as Philippe Renard and Jean-Michel Vouillamoz for their comments regarding the work during personal discussions. Finally, we are grateful to the associate editor and anonymous reviewers for their constructive comments and suggestions which have contributed to improving the quality of the manuscript.

References

Akaike, H. (1973), Information theory and an extension of the maximum likelihood principle, in *1992 Breakthroughs in Statistics: Foundations and Basic Theory*, vol. 1, edited by S. Kotz and N. L. Johnson, pp. 610–624, Springer, N. Y.

Anderson, M. P., J. S. Aiken, E. K. Webb, and D. M. Mickelson (1999), Sedimentology and hydrogeology of two braided stream deposits, *Sediment. Geol.*, *129*, 187–199, doi:10.1016/S0037-0738(99)00015-9.

Andersen, T. R., S. E. Poulsen, S. Christensen, and F. Jorgensen (2013), A synthetic study of geophysics-based moelling of groundwater flow in catchments with a buried valley, *Hydrogeol. J.*, *21*, 491–503, doi:10.1007/s10040-012-0924-5.

Ansari, A. H., and K. Alamdar (2009), Reduction to the pole of magnetic anomalies using analytic signal, *World Appl. Sci. J.*, *7*(4), 405–409.

Babiker, M., and A. Gudmundsson (2004), The effects of dykes and faults on groundwater flow in an arid land: The Red Sea Hills, Sudan, *J. Hydrol.*, *297*, 256–273, doi:10.1016/j.jhydrol.2004.04.018.

Bates, C. R., and R. Robinson (2000), Geophysical surveys for groundwater modelling of Coastal Golf Courses, paper presented at 62nd European Association of Geoscientists and Engineers Conference and Technical Exhibition, Glasgow, Scotland, 29 May–2 Jun.

Bennett, J. R. P. (1976), The Lagan Valley: Hydrogeological study, *Open File Rep.*, *57*, 105 pp., Geol. Surv. of Northern Ireland, Belfast.

Brunner, P., H.-J. Hendricks Franssen, L. Kgotlhang, P. Bauer-Gottwein, and W. Kinzelbach (2007), How can remote sensing contribute in groundwater modeling?, *Hydrogeol. J.*, *15*, 5–18, doi:10.1007/s10040-006-0127-z.

Burnham, K. P., and D. R. Anderson (2002), *Model Selection and Multimodel Inference: A Practical Information-Theoretic Approach*, 2nd ed., Springer, N. Y.

Burnham, K. P., and D. R. Anderson (2004), Multimodel inference: Understanding AIC and BIC in model selection, *Sociol. Methods Res.*, *33*(2), 261–304, doi:10.1177/0049124104268644.

Burns, C., J.-C. Comte, L. Gaffney, U. Ofterdinger, and M. Young (2010), Characterization of the effect of dyke swarms on groundwater flow in a sedimentary coastal aquifer by combined geophysical and hydrogeological modelling, Abstract H11E-0842 presented at 2010 Fall Meeting, AGU, San Francisco, Calif.

Cardwell, W. T., and R. L. Parsons (1945), Average permeabilities of heterogeneous oil sands, *Trans. Am. Inst. Min. Metall. Pet. Eng.*, *160*(1), 34–42, doi:10.2118/945034-G.

Carrera, J., and S. P. Neuman (1986), Estimation of aquifer parameters under transient and steady-state conditions: 1. Maximum Likelihood Method Incorporating Prior Information, *Water Resour. Res.*, *22*(2), 199–210, doi:10.1029/WR022i002p00199.

Chacksfield, B. C. (2010), A preliminary interpretation of Tellus airborne magnetic and electromagnetic data for Northern Ireland, *Br. Geol. Surv. Internal Rep. IR/07/041*, Br. Geol. Surv., Nottingham, U. K.

Chandler, M. A., G. Kocurek, D. J. Goggin, and L. W. Lake (1989), Effects of stratigraphic heterogeneity on permeability in eolian sandstone sequence, Page Sandstone, Northern Arizona, *Am. Assoc. Pet. Geol. Bull.*, *73*(5), 658–668.

Chen, Y., L. J. Durlofsky, M. Gerritsen, and X. H. Weh (2003), A coupled local-global upscaling approach for simulating flow in highly heterogeneous formations, *Adv. Water Resour.*, *26*, 1041–1060, doi:10.1016/S0309-1708(03)00101-5.

Comte, J.-C., and O. Banton (2007), Cross-validation of geo-electrical and hydrogeological models to evaluate seawater intrusion in coastal aquifers, *Geophys. Res. Lett.*, *34*, L10402, doi:10.1029/2007GL029981.

Comte, J.-C., O. Banton, J.-L. Join, and G. Cabioch (2010), Evaluation of effective groundwater recharge of freshwater lens in small islands by the combined modeling of geoelectrical data and water heads, *Water Resour. Res.*, *46*, W06601, doi:10.1029/2009WR008058.

Comte, J.-C., U. Ofterdinger, C. Wilson, and C. Burns (2012), Rôle hydrogéologique des dykes volcaniques au sein de l'aquifère côtier des grès de Belfast (Irlande du Nord) et implications pour la gestion de la ressource, paper presented at the Dix-huitièmes journées techniques du Comité Français d'Hydrogéologie de l'Association Internationale des Hydrogéologues, Ressources et gestion des aquifères littoraux, Cassis, France.

Cooper, M. R., H. Anderson, J. J. Walsh, C. L. Van Dam, M. E. Young, G. Earls, and A. Walker (2012), Palaoegene Alpine tectonics and Icelandic plume-related magmatism and deformation in Northern Ireland, *J. Geol. Soc.*, *169*, 29–36, doi:10.1144/0016-76492010-182.

Cronin, A. A. (2000), Groundwater flow and isotope geochemical modelling of the Triassic Sandstone aquifer, Northern Ireland, PhD thesis, Sch. of Plann. Archit. and Civ. Eng., Queen's Univ., Belfast.

Cronin, A. A., T. Elliot, Y. Tang, and R. M. Kalin (2000), Geochemical modelling and isotope studies in the Sherwood Sandstone Aquifer, Lagan Valley, Northern Ireland, in *Tracers and Modelling in Hydrogeology, Proceedings of the TraM 2000 Conference held at Liège, Belgium, IAHS Publ. 262*, edited by A. Dassargues, pp. 425–431, Int. Assoc. of Hydrol. Sci., Oxfordshire, U. K.

Cronin, A. A., J. A. C. Barth, T. Elliot, and R. M. Kalin (2005), Recharge velocity and geochemical evolution for the Permo-Triassic Sherwood Sandstone, Northern Ireland, *J. Hydrol.*, *315*, 308–324, doi:10.1016/j.jhydrol.2005.04.016.

Dagan, G. (1989), *Flow and Transport in Porous Formations*, Springer, Berlin.

Davis, J. M., and F. M. Philips (1990), A quantitative geological study of heterogeneity: Sierra Ladrones Formation, central New Mexico, in *Proceedings of the International Conference and Workshop on Transport and Mass Exchange Processes in Sand and Thermal Aquifers: Field and Modelling Studies, AECL-10308*, edited by G. Moltyaner, pp. 318–341, At. Energy of Canada Ltd., Chalk River, Ont.

de Marsily, G. (1986), *Quantitative Hydrogeology: Groundwater Hydrology for Engineers*, Academic, San Diego, Calif.

de Marsily, G., F. Delay, V. Teles, and M. T. Schafmeister (1998), Some current methods to represent the heterogeneity of natural media in hydrogeology, *Hydrogeol. J.*, *6*, 115–130, doi:10.1007/s100400050138.

de Marsily, G., F. Delay, J. Gonçalvès, P. Renard, V. Teles, and S. Violette (2005), Dealing with spatial heterogeneity, *Hydrogeol. J.*, *13*, 161–183, doi:10.1007/s10040-004-0432-3.

Dickson, N. E. M., J.-C. Comte, J. McKinley, and U. Ofterdinger (2014), Integrating geophysical data and upscaling techniques to support regional groundwater flow modelling: A practical example of the Lagan Valley, Northern Ireland. Geophysical Research Abstracts, vol. 16, presented at EGU2014, Vienna.

Doherty, J. (1994), *PEST: Model-Independent Parameter Estimation*, 3rd ed., Watermark Numer. Comput, Corinda 4075, Australia.

Duan, Q., N. K. Ajami, X. Gao, and S. Sorooshian (2007), Multi-model ensemble hydrologic prediction using Bayesian model averaging, *Adv. Water Resour.*, *30*, 1371–1386. doi:10.1016/j.advwatres.2006.11.014.

Engelhardt, L., J. G. De Aguinaga, H. Mikat, C. Schüth, and R. Liedl (2013), Complexity vs. simplicity: Groundwater model ranking using information criteria, *Ground Water*, *52*(4), 573–583, doi:10.1111/gwat.12080.

Fay, D. Q. M., M. E. Young, and A. S. D. Walker (2010), Ground magnetometer survey of dykes in Co. Down, paper presented at 53rd Irish Geological Research Meeting (IGRM), Ulster Museum, Belfast.

Fleckenstein, J. H., and G. E. Fogg (2008), Efficient upscaling of hydraulic conductivity in heterogeneous alluvial aquifers, *Hydrogeol. J.*, *16*, 1239–1250, doi:10.1007/s10040-008-0312-3.

Foglia, L., S. W. Mehl, M. C. Hill, P. Perona, and P. Burlando (2007), Testing alternative ground water models using cross-validation and other methods, *Ground Water*, *45*(5), 627–641, doi:10.1111/j.1745–6584.2007.00341.x.

Friedel, M. J., O. A. Souza Filho, F. Iwashita, A. M. Silva, and S. Yoshinaga (2012), Data-driven modeling for groundwater exploration in fractured crystalline terrain, northeast Brazil, *Hydrogeol. J.*, *20*, 1061–1080, doi:10.1007/s10040-012-0855-1.

Fu, L., K. L. Milliken, and J. M. Sharp Jr. (1994), Porosity and permeability variations in fractured and liesegang-banded Breathitt sandstones (Middle Pennsylvanian), eastern Kentucky: Diagenetic controls and implications for modeling dual-porosity systems, *J. Hydrol.*, *154*(1–4), 351–381, doi:10.1016/0022-1694(94)90225-9.

Gedeon, M., I. Wemaere, and S. Labat (2012), Characterization of groundwater flow in the environment of the boom clay formation, *Phys. Chem. Earth*, *36*, 1486–1495, doi:10.1016/j.pce.2011.07.089.

Gondwe, B. R. N., S. Lerer, S. Stisen, L. Marín, M. Rebolledo-Vieyra, G. Merediz-Alonso, and P. Bauer-Gottwein (2010), Hydrogeology of the south-eastern Yucatan Peninsula: New insights from water level measurements, geochemistry, geophysics and remote sensing, *J. Hydrol.*, *389*, 1–17, doi:10.1016/j.jhydrol.2010.04.044.

Grauch, V. J. S., M. R. Hudson, and S. A. Minor (2001), Aeromagnetic expression of faults that offset basin fill, Albuquerque basin, New Mexico, *Geophysics*, *66*(3), 707–720, doi:10.1190/1.1444961.

Hartley, J. J. (1935), The underground water resources of Northern Ireland, paper presented at Belfast and District Association, Inst. of Civ. Eng. (Northern Ireland Assoc.), Belfast.

Hartmann, S., and P. McConvey (2007), Surface and groundwater quality: Meeting new standards, paper presented at The Tellus Conference on Geoscience for decision making, GSNI, Belfast.

Herckenrath, D., G. Fiandaca, E. Auken, and P. Bauer-Gottwein (2013), Sequential and joint hydrogeophysical inversion using a field-scale groundwater model with ERT and TDEM data, *Hydrol. Earth Syst. Sci.*, *17*, 4043–4060, doi:10.5194/hess-17-4043-2013.

Hill, M. C. (2006), The practical use of simplicity in developing ground water models, *Ground Water*, *44*(6), 775–781, doi:10.1111/j.1745–6584.2006.00227.x.

Hill, M. C., and C. R. Tiedeman (2007), *Effective Groundwater Model Calibration—With Analysis of Data, Sensitivities, Predictions, and Uncertainty*, John Wiley, Hoboken, N. J.

Hurvich, C. M., and C.-L. Tsai (1989), Regression and time series model selection in small samples, *Biometrika*, *76*(2), 297–307, doi:10.1093/biomet/76.2.297.

Hurvich, C. M., and C.-L. Tsai (1995), Model selection for extended quasi-likelihood models in small samples, *Biometrics*, *51*, 1077–1084, doi:10.2307/2533006.

Kalin, R. M., and C. Roberts (1997), Groundwater resources in the Lagan Valley Sandstone aquifer, Northern Ireland, *J. Chart. Inst. Water Environ. Manage.*, *11*(2), 133–139, doi:10.1111/j.1747-6593.1997.tb00104.x.

Kirsch, R. (Ed.) (2006), *Groundwater Geophysics: A Tool for Hydrogeology*, 2nd ed., Springer, Berlin, doi:10.1007/978-3-540-88405-7.

Klingbeil, R., S. Kleineidam, U. Asprion, T. Aigner, and G. Teutsch (1999), Relating lithofaces to hydrofacies: Outcrop-based hydrogeological characterisation of quaternary gravel deposits, *Sediment. Geol.*, *129*, 299–310, doi:10.1016/S0037-0738(99)00067-6.

Koch, M., and P. M. Mather (1997), Lineament mapping for groundwater resource assessment: A comparison of digital Synthetic Aperture Radar (SAR) imagery and stereoscopic Large Format Camera (LFC) photographs in the Red Sea Hills, Sudan, *Int. J. Remote Sens.*, *18*(7), 1465–1482, doi:10.1080/014311697218223.

Koltermann, C. E., and S. M. Gorelick (1996), Heterogeneity in sedimentary deposits: A review of structure-imitating, process-imitating, and descriptive approaches, *Water Resour. Res.*, *32*(9), 2617–2658, doi:10.1029/96WR00025.

Mabey, D. R. (1974), Magnetic methods, in *Application of Surface Geophysics to Ground-Water Investigations, Techniques of Water-Resources Investigations of the United States Geological Survey*, by edited by A. A. R. Zohdy, G. P. Eaton, and D. R. Mabey, chap. D1, pp. 107–115, U. S. Gov. Print. Off., Denver.

Manning, P. I., J. H. Robbie, and H. E. Wilson (1970), *Geology of Belfast and the Lagan Valley: Memoir for 1:63360 Geological Sheet 36 (Northern Ireland)*, 2nd ed., H. M. Stationery Off., Belfast.

Mariethoz, G., P. Renard, and J. Straubhaar (2010), The direct sampling method to perform multiple-point geostatistical simulations, *Water Resour. Res.*, *46*, W11536, doi:10.1029/2008WR007621.
Matheron, G. (1967), *Éléments pour une théorie des milieux poreux*, Masson, Paris.
McCabe, M. (2008), *Glacial Geology and Geomorphology: The Landscapes of Ireland*, Dunedin Academic, Edinburgh, U. K.
McKinley, J. M., R. H. Worden, and A. H. Ruffell (2001), Contact diagenesis: The effect of an intrusion on reservoir quality in the Triassic Sherwood Sandstone Group, Northern Ireland, *J. Sediment. Res.*, *71*(3), 484–495, doi:10.1306/2DC40957-0E47-11D7-8643000102C1865D.
McNeill, G. W., A. A. Cronin, Y. Yang, T. Elliot, and R. M. Kalin (2000), The Triassic Sherwood Sandstone Aquifer in Northern Ireland: Constraint of a groundwater flow model for resource management, in *Groundwater in The Celtic Regions: Studies in Hard Rock and Quaternary Hydrogeology, Geol. Soc. Spec. Publ. 182*, edited by N. S. Robins and B. D. Misstear, pp. 179–190, Geol. Soc., Bath, U. K.
Mitchell, W. I. (2004), Triassic, in *The Geology of Northern Ireland; Our Natural Foundation*, 2nd ed., edited by W. I. Mitchell, pp. 133–144, Geol. Surv. of Northern Ireland, Belfast.
Morel, E. H., and R. S. Wikramaratna (1982), Numerical modelling of groundwater flow in regional aquifers dissected by dykes, *Hydrol. Sci. J.*, *27*(1), 63–77, doi:10.1080/02626668209491086.
Noetinger, B., V. Artus, and G. Zargar (2005), The future of stochastic and upscaling methods in hydrogeology, *Hydrogeol. J.*, *13*, 184–201, doi:10.1007/s10040-004-0427-0.
Nyborg, M., J. Berglund, and C.-A. Triumf (2007), Detection of lineaments using airborne laser scanning technology: Laxemar-Simpevarp, Sweden, *Hydrogeol. J.*, *15*, 29–32, doi:10.1007/s10040-006-0134-0.
Okazaki, K., et al. (2011), Airborne electromagnetic and magnetic surveys for long tunnel construction design, *Phys. Chem. Earth*, *36*, 1237–1246, doi:10.1016/j.pce.2011.05.008.
Parker, A. H., L. J. West, N. E. Odling, and R. T. Bown (2010), A forward modeling approach for interpreting impeller flow logs, *Ground Water*, *48*(1), 79–91, doi:10.1111/j.1745-6584.2009.00600.x.
Poeter, E. P., and D. R. Anderson (2005), Multimodel ranking and inference in ground water modeling, *Ground Water*, *43*(4), 597–605, doi:10.1111/j.1745-6584.2005.0061.x.
Price, M. (1996), *Introducing Groundwater*, Chapman and Hall, London, U. K.
Rasmussen, P., T. O. Sonnenborg, G. Goncear, and K. Hinsby (2013), Assessing impacts of climate change, sea level rise, and drainage canals on saltwater intrusion to coastal aquifer, *Hydrol. Earth Syst. Sci.*, *17*, 421–443, doi:10.5194/hess-17-421-2013.
Renard, P. (2007), Stochastic hydrogeology: What professionals really need?, *Ground Water*, *45*(5), 531–541, doi:10.1111/j.1745-6584.2007.00340.x.
Renard, P., and G. de Marsily (1997), Calculating equivalent permeability: A review, *Adv. Water Resour.*, *20*(5–6), 253–278, doi:10.1016/S0309–1708(96)00050-4.
Renard, P., G. Le Loc'h, E. Ledoux, G. de Marsily, and R. Mackay (2000), A fast algorithm for the estimation of the equivalent hydraulic conductivity of heterogeneous media, *Water Resour. Res.*, *36*(12), 3567–3580, doi:10.1029/2000WR900203.
Robins, N. S. (1996), *Hydrogeology of Northern Ireland, Environment and Heritage Service*, HMSO for the Br. Geol. Soc., London, U. K.
Robinson, D. A., et al. (2008), Advancing process-based watershed hydrological research using near-surface geophysics: A vision for, and review of, electrical and magnetic geophysical methods, *Hydrol. Processes*, *22*, 3604–3635, doi:10.1002/hyp.6963.
Rubin, Y., and S. S. Hubbard (2005), *Hydrogeophysics, Water Science and Technology Library*, vol. 50, Springer, Dordrecht, Netherlands.
Sandberg, S. K., L. D. Slater, and R. Versteeg (2002), An integrated geophysical investigation of the hydrogeology of an anisotropic unconfined aquifer, *J. Hydrol.*, *267*, 227–243, doi:10.1016/S0022–1694(02)00153-1.
Sander, P. (2007), Lineaments in groundwater exploration: A review of applications and limitations, *Hydrogeol. J.*, *15*, 71–74, doi:10.1007/s10040-006-0138-9.
Schwartz, F. W., and H. Zhang (2003), *Fundamentals of Groundwater*, John Wiley, N. Y.
Sharp, J. M., Jr., L. Fu, P. Cortez, and E. Wheeler (1994), An electronic minipermeameter for use in the field and laboratory, *Ground Water*, *32*(1), 41–46, doi:10.1111/j.1745-6584.1994.tb00609.x.
Siemon, B., A. Steuer, A. Ullmann, M. Vasterling, and W. Voß (2011), Application of frequency-domain helicopter-borne electromagnetics for groundwater exploration in urban areas, *Phys. Chem. Earth*, *36*, 1373–1385, doi:10.1016/j.pce.2011.02.006.
Singh, A., S. Mishra, and R. Ruskauff (2010), Model averaging techniques for quantifying conceptual model uncertainty, *Ground Water*, *48*(5), 701–715, doi:10.1111/j.1745-6584.2009.00642.x.
Solomon, S., and F. Quiel (2006), Groundwater study using remote sensing and Geographic Information Systems (GIS) in the central highlands of Eritrea, *Hydrogeol. J.*, *14*, 729–741, doi:10.1007/s10040-005-0477-y.
Strebelle, S. (2002), Conditional simulation of complex geological structures using multiple-points statistics, *Math. Geol.*, *34*(1), 1–21, doi:10.1023/A:1014009426274.
Verduzco, B., J. D. Fairhead, C. M. Green, and C. MacKenzie (2004), New insights into magnetic derivatives for structural mapping, *Leading Edge*, *23*(2), 116–119.
Webb, E. K., and M. P. Anderson (1996), Simulation of preferential flow in three-dimensional, heterogeneous conductivity fields with realistic internal architecture, *Water Resour. Res.*, *32*(3), 533–545, doi:0043-1397/96/95WR-033995.
Wen, X.-H., and J. J. Gómez-Hernández (1996), Upscaling hydraulic conductivities in heterogeneous media: An overview, *J. Hydrol.*, *183*(1–2), 9–32, doi:10.1016/S0022-1694(96)80030-8.
Wen, X., L. Durlofsky, and M. Edwards (2003), Use of border regions for improved permeability upscaling, *Math. Geol.*, *35*(5), 521–547, doi:10.1023/A:1026230617943.
Wen, X. H., Y. Chen, and L. J. Durlofsky (2006), Efficient 3D implementation of local-global upscaling for reservoir simulation, *Soc. Petrol. Eng. J.*, *11*(4), 443–453, doi:10.2118/92965-PA.
Wiener, O. (1912), Abhandlungen der mathematisch, *Physischen Klasse Koniglichen Sachsischen Ges. Wiss.*, *32*(6), 509.
Wilson, C. (2011), Analysis of the effect of volcanic dykes on groundwater flow in the Sherwood sandstone aquifer, Impacts on piezometry, salinity, and attenuation of the tidal signal, MSc thesis, Sch. of Plann. Archit. and Civ. Eng., Queen's Univ., Belfast.
Wilson, E. M. (1990), *Engineering Hydrology*, 4th ed., Palgrave Macmillan, Hampshire, U. K.
Yang, Y. S., A. A. Cronin, T. Elliot, and R. M. Kalin (2004), Characterizing a heterogeneous hydrogeological system using groundwater flow and geochemical modelling, *J. Hydraul. Res.*, *42*(extra issue), 147–155, doi:10.1080/00221680409500058.
Ye, M., P. D. Meyer, and S. P. Neuman (2008), On model selection criteria in multimodel analysis, *Water Resour. Res.*, *44*, W03428, doi:10.1029/2008WR006803.
Ye, M., K. F. Pohlmann, J. B. Chapman, G. M. Pohll, and D. M. Reeves (2010), A model-averaging method for assessing groundwater conceptual model uncertainty, *Ground Water 48*, 716–728, doi:10.1111/j.1745-6584.2009.00633.x.